Investigation on the Strain Effect on the Behaviour of Laminated Veneer Lumber Timber Connections

Author

Cheng, Xinyi, Gilbert, Benoit P, Lyu, Chunhao, Guan, Hong

Published

2024

Conference Title

Proceedings of the 7th International Conference on Geotechnics, Civil Engineering and Structures, CIGOS 2024, 4-5 April, Ho Chi Minh City, Vietnam

Version

Accepted Manuscript (AM)

DOI

10.1007/978-981-97-1972-3_54

STRAIN RATE EFFECT ON THE EMBEDMENT MECHANICAL PROPERTIES AND FRACTURE BEHAVIOUR OF SOFTWOOD LAMINATED VENEER LUMBERS – IMPLICATIONS TO TIMBER CONNECTIONS

Xinyi Cheng(1), Benoit P. Gilbert(2), Chunhao Lyu(3), Hong Guan(4)

(1) School of Engineering and Built Environment, Gold Coast campus, Griffith University, QLD, Australia
Email: chelsea.cheng@multinail.com
(2) School of Engineering and Built Environment, Gold Coast campus, Griffith University, QLD, Australia
Corresponding author: b.gilbert@griffith.edu.au
(3) School of Engineering and Built Environment, Gold Coast campus, Griffith University, QLD, Australia
Email: c.lyu@griffith.edu.au
(4) School of Engineering and Built Environment, Gold Coast campus, Griffith University, QLD, Australia
Email: h.guan@griffith.edu.au

Abstract: This paper experimentally investigates the influence of the strain rate experienced during earthquake and progressive collapse events on mechanical properties affecting the design of softwood Laminated Veneer Lumbers timber connections. The parallel and perpendicular to grain embedment stiffness and strength, the tension strength perpendicular to grain, and the Mode I and II fracture energies were examined under four levels of strain rates. Results showed that the embedment stiffness and strength increased by up to 35% from the quasi-static to dynamic strain rates while the embedment ductility decreased by up to 17%. The fracture energies and tension strength perpendicular to grain were found to be mostly insensitive to the investigated range of strain rates. Furthermore, the influence of the strain rate on the behaviour of timber connections is analysed and discussed by (1) using the experimental data in the Eurocode 5 design equations for single and double shear connections and (2) quasi-statically and dynamically testing one connection type with two different fastener spacings. Results showed that for the connections investigated, the dynamic strength can be up to 30% higher than the quasi-static one, however, the dynamic ductility of the connections can be reduced substantially by up to 32.5%.

KEYWORDS: Timber connection, Strain rate effect, Fracture energy, Tension perpendicular to grain, Embedment strength

INTRODUCTION

The last few decades have seen the emergence of tall mass timber buildings (Harte, 2017, Kuzmanovska, et al., 2018), which have reached unprecedented heights. At the time of writing this paper, the highest built mass timber building, Ascent in the US, reaches 86.5 m in height. Nevertheless, other projects, such as the Rocket&Tigerli in Switzerland, are set to beat this record. As mass timber buildings are becoming taller, it follows that correctly understanding their dynamic response is essential, as they may experience extreme dynamic events during their lifetime, including earthquakes or accidental loads leading to localised damage of critical load bearing element(s). These two events may potentially trigger progressive collapse, with the initial damage propagating throughout the building, in a chain reaction, leading to the partial or entire collapse the structural system (Ellingwood, et al., 2007). Timber connections tested for robustness by Cheng, et al. (2021) showed that failure may dynamically occur at significantly smaller deformations than those observed under quasi-static loading (Lyu, et al., 2020). This difference has profound consequences on the design of mass timber buildings as the ductility level assumed in current design guidelines (AS 1720.1, 2010, EN 1995-1-1, 2004) may not be reached dynamically. As connections play an important role in the robustness of mass timber buildings (Brühl, et al., 2011, Jorissen, et al., 2011), accurately predicting the dynamic behaviour of these connections therefore requires attention to design and construct safe buildings under dynamic loading.

This paper therefore investigates the influence of the strain rate experienced during earthquake and progressive collapse events on softwood Laminated Veneer Lumbers (LVL) connections with a focus on (1) the mechanical properties affecting the structural response of timber connections and (2) the behaviour of timber connections. Key mechanical properties influencing the ductile and brittle failure modes of timber connections were investigated. They consisted of the embedment stiffness and strength, parallel and perpendicular to grain, of a 16 mm diameter dowelled connection, of the tension strength perpendicular to grain, and Mode I and II fracture energies of the material. These properties were quantified under four levels of strain rates, from reaching failure in 300 sec (quasi-static) to 0.3

sec (dynamic - earthquakes and progressive collapse events (Bischoff, et al., 1991)). Regarding the behaviour of the timber connections and to further capture the critical influence of the strain rate on their structural response, the capacities of timber-to-timber dowelled connections in single and double shear were calculated by inputting the characteristic embedment strength values obtained from the experimental data into the Eurocode 5 (EN 1995-1-1, 2004) design equations. In addition, one bolted connection type, with two different fastener spacings, was tested quasi-statically and dynamically.

In the paper, an overview of the existing work examining the influence of the strain rate on the mechanical properties of timber is first presented. Second, the methodology is introduced for both the investigation on the behaviour of the material itself and the associated timber connections. Finally, the results and their implications on the design of timber connections under dynamic loading are discussed.

OVERVIEW OF EXISTING WORK

General

Investigations on the influence of the strain rate on the strength and stiffness of timber are scarce and have principally been performed in compression and under high strain rate using the Split Hopkinson Pressure Bar (SHPB) method (Sreenivasan, et al., 2001). Such tests result in strain rates corresponding to the ones experienced during blast events (Bischoff, et al., 1991), i.e., more than 10^4 higher than earthquake and progressive collapse strain rates. Little investigations have been performed in shear (Keeton, 1968), bending (Jacques, et al., 2014, Keeton, 1968, Wood, 1951) and tension. Therefore, the following subsection focuses and summarises the key studies and results in compression.

With respect to the relationship between the fracture properties and strain rate, work has been performed on measuring both the fracture toughness (or critical energy release rate, with the critical energy release rate being directly correlated to the fracture toughness (Knott, 1973)) and fracture energy. Subsection *Fracture properties* presents the results on these key studies showing that different trends are encountered in the literature.

Strength and stiffness in compression

Xie, et al. (2020) tested the parallel to grain compressive responses of small cubes of three species of softwoods (spruce, Dhorian larch and pine) under strain rates varying from 10^{-4} sec^{-1} (i.e., quasi-static and failure in about 250 sec) to 10^{-1} sec^{-1} (i.e., failure in about 0.25 sec). Results showed an increased in strength of about 20% from low to high strain rates. For higher strain rates, Widehammar (2004) studied the dynamic compressive strengths, parallel and perpendicular to grain, on small cubes cut from the sapwood of a single spruce log. Strength rates ranging from 8×10^{-3} sec^{-1} (i.e., failure in about 4-6 sec) to 1,000 sec^{-1} (i.e., failure in about 5×10^{-5} sec) were examined. The effect of the strain rate on the strength was found to be higher parallel to than perpendicular to grain, with the tangential strength increasing by about 20% from strain rates of 8×10^{-3} sec^{-1} to 17 sec^{-1}, compared to an increase of about 50% parallel to grain. Similar results were obtained for (1) balsa, pine, redwood and oak under impact velocity up to 300 m/sec by Reid, et al. (1997), (2) beech and spruce specimens under strain rate up to 600 sec^{-1} by Wouts, et al. (2016), and (3) pine, birch and lime specimens under strain rate up to 5,000 sec^{-1} (Bragov, et al., 1997). Other similar studies include those of Gilbertson, et al. (2013) and Zhou, et al. (2020).

Fracture properties

Using double cantilever beam specimens made from spruce, with a RL (Radial – Longitudinal) crack system, Mai (1975) found that fracture toughness decreases with the crack speed propagation, therefore the resistance to crack propagation decreases with increased crack speed. Crack speed propagations from 0.1 mm/s to 10 mm/s were analysed. Nadeau, et al. (1982) investigated the fracture properties on notched Douglas fir beams at various strain rates, ranging from 2.6×10^{-3} MPa/sec to 68.9 MPa/sec, and with the specimens orientated to promote cracking in the LT (Longitudinal – Tangential) system. The strain rate was shown to have little influence on the fracture strength and fracture toughness. Using double edge notched specimens, Schniewind, et al. (1971) measured the fracture toughness in the TR (Tangential – Radial) crack system to have increased by 28% when the strain rate changed from 2.3×10^{-3} min^{-1} to 2.3×10^{-2} min^{-1}. Conrad, et al. (2003) also suggested that the fracture toughness of solid wood increases with the strain rate.

For fracture energy, Vasić, et al. (2009) performed Mode I fracture tests in the RL crack system using double cantilever Norway spruce sawn beams. The loading speeds were varied to reach failure between 1 hour to 0.03 sec. The fracture energy increased up to failure occurring in 18-36 sec and then decreased.

It is worth mentioning that, while for perfectly brittle materials, the critical energy release rate and the fracture energy are equal (Ardalany, et al., 2012), this is not the case for wood. Wood behaves as a quasi-brittle material, with a fracture process zone not small enough for the material to behave in a brittle manner (Stanzl-Tschegg, et al., 2009, Vasic, et al., 2002b), resulting in significant differences between the critical energy release rates and the fracture energies for both sawn timber and Engineered Wood Products (Ardalany, et al., 2012, Vasic, et al., 2002a, Vasic, et al., 2002b). When modelling with techniques suitable for quasi brittle materials, such as Continuous Damage Mechanics (CDM) or Cohesive Zone Modelling (CZM), Mode I and II fracture energies are needed as input properties, along with crack initiation stresses. Examples of CDM and CZM for timber modelling can be found in Gilbert, et al. (2020), Cheng, et al. (2022), Gharib, et al. (2017), Nouri, et al. (2019) and Xu, et al. (2009).

MATERIALS AND METHODS

Mechanical properties

Material, loading rates and other parameters

All tested specimens were manufactured from HySPAN LVL structural products which were assembled from either Radiata pine (*Pinus radiata*) or Douglas fir (*Pseudotsuga menziesii*) veneers, with no cross layers (Carter Holt Harvey, 2015). The specimens were conditioned at 20°C and 65%

relative humidity before testing. Moisture samples were cut and weighed from selected samples immediately after testing to determine the moisture content at the time of testing following the oven-dry methodology specified in the AS/NZS 1080.1 (2012), resulting in an average moisture content of 10.9%, with a coefficient of variation (CoV) of 2.24%.

For all material properties presented in the following subsections, samples were tested under four levels of strain rates to target failure in 300 sec, 30 sec, 3 sec, and 0.3 sec, allowing detailed observation of the evolution of the relationships between strain rates and the studied material properties. The loading speeds were determined from pre-tests to best achieve the targeted times to failure. For each loading speed and material property, 20 tests were performed to ensure the reliability of the results. The samples were cut from 20 different LVL boards, with each sample per set of 20 cut from a different board so not to be bias towards one board. In total, 400 material tests were conducted.

One-way analysis of variance (ANOVA) was used to determine whether there were statistically significant differences between the mean results from different strain rates. Characteristic values were also calculated based on the performed number of tests following the methodology in Clause 3.2 of the European standard EN 14358 (2016), assuming lognormal distributions.

The tests were performed following the best practices for structural testing outlined by Gilbert, et al. (2022).

Embedment properties

As the embedment strengths, both parallel and perpendicular to grain, are typical key parameters for the design of connections in standards, such as the Eurocode 5 (EN 1995-1-1, 2004), the influence of the strain rate on the embedment behaviour was determined herein following the half-hole embedment tests in the ASTM D5764 − 97a (2018). Tests were performed using 16 mm non coated steel dowels. Each half-hole LVL specimen was 120 mm wide, 70 mm high and 45 mm thick, with a 16 mm diameter half-hole on the top surface, as shown in Figure 1. Each hole was drilled on a milling machine using a universal drill bit.

Before testing, each sample was positioned in the middle of a fixed bottom loading platen. A loading block, thinner than the dowel, was welded on top of it, to load the specimens through a top platen mounted on a spherical seat, therefore ensuring the uniform application of the load. All tests were conducted in displacement control in a 100 kN Instron universal testing machine. The displacement of the dowel was measured as the average reading of two laser displacement transducers, mounted on the bottom loading platen, aiming at targets that were glued symmetrically to both ends of the dowel. The test set-up is shown in Figure 2.

To ensure full contact of the dowel with the specimens and the same initial conditions for all specimens, before each test, each sample was preloaded to 3 kN and then unloaded to 0.3 kN. Tests were terminated when either the dowel displacement reached 7 mm or a significant load drop (more than 30% of the maximum load) was encountered.

The embedment stress σ_{emb} was calculated from the applied load P, divided by the measured thickness t of the sample and dowel diameter d as,

$$\sigma_{emb} = \frac{P}{td} \tag{1}$$

For each test, the embedment stress-displacement curve was used to evaluate the following values, which are illustrated for both loading parallel and perpendicular to grain in Figure 3:

- Time to failure T_f defined as the time when the dowel displacement reached 5 mm, as per EN 383 (2007), or the load dropped by 10% of the maximum load, whichever came first.
- Elastic stiffness K_{el} calculated by performing a linear regression on the curve between 10% and 40% of the maximum stress.
- Yield stress $f_{y,5\%}$ defined as in ASTM D5764 − 97a (2018), either as the stress at which a line of stiffness K_{el}, offset by a deformation of 5% of the dowel diameter, intersects with the stress-displacement curve or the maximum stress if the line intersects the curve after reaching the maximum stress.

- Embedment strength f_{emb} obtained either as the stress at a 5 mm displacement or the maximum stress if reached before a 5 mm displacement (EN 383, 2007).
- Ductility Δ which was defined as the displacement at the time of failure. Note that the ductility was only calculated for loading parallel to grain because no load drop was observed for loading perpendicular to the grain.

Fracture energy (Mode I)

The test set-up proposed by Ardalany, et al. (2012), improved from Larsen, et al. (1990), was used herein to examine the influence of the strain rate on the Mode I fracture energy, with a TL (Tangential – Longitudinal) crack system, which is shown in Figure 4. As discussed in Section *Overview of existing work*, the fracture energies are required input to model the crack propagation in timber structures and therefore timber connections.

The samples had nominal dimensions of 100 mm wide × 100 mm high × 45 mm thick. They contained one 3.5 mm thick × 60 mm deep groove to imitate fracture in the middle of the samples and two side notches, all of which were cut along the grain direction, as shown in Figure 5. The samples were held by two steel arms connected to the side notches. The assembly was simply supported, with the steel arms cantilevered past the supports and counterbalanced by weights so as not to apply gravity load to the samples. Load was applied to the samples at mid-span by a 500 kN capacity MTS universal testing machine, in a three-point bending arrangement, through a steel half-round. As the applied load was relatively small compared to the load cell of the testing machine, a 2.5 kN load cell was inserted between the loading half-round and the testing machine to accurately measure the load. Each sample was preloaded to 10 N and unloaded to 1 N before testing to ensure full contact between the steel half-round and the specimen. Each sample was subsequently tested until the load dropped by 95% of the maximum applied load.

For each test, the applied stress was calculated as the ratio of the applied load to the vertical measured cross-sectional area above the 60 mm deep groove. Displacement was recorded as the stroke of the testing machine. The following values were calculated for each sample and are illustrated in Figure 6.

- Time to failure T_f defined as the time from the beginning of the test to a decrease in the applied load of 95% of its maximum value.
- Maximum stress σ_{max} defined as the maximum stress value being reached.
- Mode I Fracture energy G_{fI} defined as the area under the stress-displacement curve from the origin until a decrease in the applied stress of 95% of σ_{max}.

Fracture energy (Mode II)

The test set-up from Franke, et al. (2014) was adopted herein to investigate the influence of the strain rate on the Mode II fracture energy, with a TL crack system. The samples had the same overall dimensions as those used for Mode I (i.e., 100 mm wide × 100 mm high × 45 mm thick) and are shown in Figure 7. Each sample had two 5 mm thick × 60 mm deep grooves cut along the grain direction, as shown in the figure. The bottom ends of the samples between the outside faces to the grooves were supported by 40 mm thick steel plates, as shown in Figure 8. The load was uniformly applied by a 100 kN Instron universal testing machine to the top of the samples through a 40 mm thick steel plate positioned between the two grooves to trigger shear failure. The same loading protocol as for the Mode I fracture tests was followed. The displacement was recorded as the stroke displacement of the testing machine.

The evaluation criteria were the same as those applied in Mode I (i.e., time to failure T_f, maximum applied stress σ_{max} and Mode II fracture energy G_{fII}), with the cross-section area used to calculate the stress equal to the sum of the measured vertical cross-section area above the two grooves.

Tension perpendicular to grain

The tension perpendicular to the grain is a key parameter for crack initiation and was evaluated herein under various strain rates following the guidance in the ASTM D143-14 (2014). While provided for small clear timber specimens, this methodology was also successfully applied to LVL samples (Ardalany, et al., 2011, Gilbert, et al., 2018, McGavin, et al., 2019). The overall dimensions for each sample, shown in Figure 9, were 65 mm wide, 50 mm high and 45 mm thick. Two 25 mm diameter holes at a centre-to-centre distance of 50 mm were drilled so that the samples could be attached to the test rig and tension failure triggered at the location of the smallest cross-sectional area. The test set-up, which is shown in Figure 10, consisted of two custom-made pieces that fit the shape of the samples which were clamped to the jaws of a 30 kN Instron universal testing machine. Before each test, the samples were preloaded to 200 N then unloaded to 20 N so that the test rig was in full contact with the samples but did not cause any damage. Each sample was then loaded till failure.

For each test, the stress was calculated as the ratio of the applied load to the measured smallest cross-sectional area of the sample. The following metrics were calculated for each sample:

- Time to failure T_f, defined as the time from the beginning of the test until reaching the maximum load.
- Tensile strength $f_{t,90}$, obtained as the maximum applied stress.

Timber connections

Design equations in Eurocode

To apprehend the influence of the strain rate on connection design, the capacity of timber-to-timber dowelled connections in single (Figure 11 (a)) and double (Figure 11 (b)) shear was calculated in this subsection using the Eurocode 5 (EN 1995-1-1, 2004) design equations. Even if the strain rate negatively influences the connection ductility, as later seen in the results section, it was implicitly assumed that enough ductility can develop for the European Yield model equations (Johansen, 1949) used in the Eurocode 5 to be valid. Per dowel, the capacity $F_{v,Rk}$ of a connection in single shear is given as the minimum of Eq. (2) to Eq. (7),

$$f_{h,1,k}t_1d \tag{2}$$

$$f_{h,2,k}t_2d \tag{3}$$

$$\frac{f_{h,1,k}t_1d}{1+\beta}\left[\sqrt{\beta+2\beta^2\left[1+\frac{t_2}{t_1}+\left(\frac{t_2}{t_1}\right)^2\right]+\beta^3\left(\frac{t_2}{t_1}\right)^2}-\beta\left(1+\frac{t_2}{t_1}\right)\right] \tag{4}$$

$$1.05\frac{f_{h,1,k}t_1 d}{2+\beta}\left[\sqrt{2\beta(1+\beta)+\frac{4\beta(2+\beta)M_{y,Rk}}{f_{h,1,k}dt_1^2}}-\beta\right] \tag{5}$$

$$1.05\frac{f_{h,1,k}t_2 d}{1+2\beta}\left[\sqrt{2\beta^2(1+\beta)+\frac{4\beta(1+2\beta)M_{y,Rk}}{f_{h,1,k}dt_2^2}}-\beta\right] \tag{6}$$

$$1.15\sqrt{\frac{2\beta}{1+\beta}}\sqrt{2M_{y,Rk}f_{h,1,k}d} \tag{7}$$

where, t_1 and t_2 are the thicknesses of the timber members as shown in Figure 11, d is the dowel diameter, β is the ratio between the embedment strength of the members defined as,

$$\beta=\frac{f_{h,2,k}}{f_{h,1,k}} \tag{8}$$

where, $f_{h,1,k}$ and $f_{h,2,k}$ are the characteristic embedment strengths of the dowel in Members 1 and 2, respectively. In Eqs. (5-7), $M_{y,Rk}$ is the characteristic fastener yield moment determined as,

$$M_{y,Rk}=0.3f_{u,k}d^{2.6} \tag{9}$$

where, $f_{u,k}$ is the characteristic tensile strength of the dowel. The failure modes in Eqs. (2) to (7) for a connection in single shear are illustrated in Figure 12.

For a connection in double shear, the capacity $F_{v,Rk}$ per dowel and per shear plane is given in the Eurocode 5 (EN 1995-1-1, 2004) as the minimum of Eqs. (2), (5), (7) and,

$$0.5f_{h,2,k}t_2 d \tag{10}$$

The failure modes in Eqs. (2), (5), (7) and (10) for a connection in double shear are illustrated in Figure 13.

Analyses were performed with t_1 set at 45 mm and t_2 varying from 20 to 90 mm. Additionally, Member 2 was taken either loaded parallel or perpendicular to the grain, while Member 1 was only considered to be loaded parallel to the grain. The characteristic embedment strengths for each strain rate, $f_{h,1,k}$ and $f_{h,2,k}$, were taken from the experimental values and provided in the results section. The characteristic tensile strength of the 16 mm diameter dowel $f_{u,k}$ was taken as 460 MPa (Rothoblaas, 2019). d was equal to 16 mm as per in the experiment tests.

Experimental tests

To further explore the influence of the strain rate on the connection behaviour, one type of double shear bolted connection, with outer steel plates, was quasi-statically and dynamically experimentally tested. The connection type is shown in Figure 14 and consisted of a 45 mm thick × 150 mm wide hySPAN LVL (Carter Holt Harvey, 2015) sandwiched between two 10 mm thick steel plates of grade 250 (AS 4100, 2020). Each connection had four M8 bolts of grade 4.6, with steel washers and torqued at 10 N·m. The shank of the bolts was 55 mm long, so that the timber element was not in contact with the thread. 9 mm diameter holes were drilled into the timber to fit the bolts. Two different bolt configurations, corresponding to two different bolt spacings, were investigated, as shown in Figure 14 (a) for Configuration #1 and Figure 14 (b) for Configuration #2. For this type of connection, the Eurocode 5 (EN 1995-1-1, 2004) predicts that the connection would fail due to plastic hinges developing in the bolts and local bearing of the timber member.

The test set-up is illustrated in Figure 15. The steel plates were connected to the bottom jaw of a 500 kN universal MTS testing machine and the timber element was connected to the top jaw with an overdesigned connection. A tension load was applied to reach the maximum load in either 300 sec (quasi-statically) or 0.3 sec (dynamically). Two laser transducers, each positioned symmetrically on both sides of the connection, recorded the relative displacement (taken as the average of the two transducers) between the steel plates and the LVL. Per configuration and loading speed, three tests were performed for repeatability. Before each test, the connection was preloaded to 20 kN and unloaded to 0 kN to have all elements in contact.

For each test, the following metrics were measured for each sample:

- Maximum load F_{max}.

- Time to failure T_f, defined as the time from the beginning of the test until reaching the maximum load.
- Ductility Δ which was defined as the displacement at the time of failure.

RESULTS AND DISCUSSION

Mechanical properties

Embedment properties

The embedment stress-displacement curves under all strain rates are shown in Figure 16 and Figure 17 for loading parallel and perpendicular to the grain, respectively. Loading speeds and average failure times, elastic stiffness, yield stresses, embedment strengths and ductility values, with associated CoV, are given in Table 1. The calculated characteristic embedment strength for each strain rate and loading direction is also provided in the table.

The embedment properties in both parallel and perpendicular to grain directions were found to be sensitive to strain rate changes, with the one-way ANOVA showing that there was a statistically significant difference between groups for both the embedment strength f_{emb} and stiffness K_{el} values. The one-way ANOVA resulted in (1) parallel to grain: $F(3,76) = 32.35$, $p = 1.4\times10^{-13}$ and $F(3,76) = 2.94$, $p = 0.038$ for f_{emb} and K_{el}, respectively, and (2) perpendicular to grain: $F(3,76) = 43.88$, $p = 1.4\times10^{-16}$ and $F(3,76) = 42.25$, $p = 3.6\times10^{-16}$ for f_{emb} and K_{el}, respectively.

Both the embedment strength and stiffness increased with the strain rate. When comparing results for failure occurring between 300 sec and 0.3 sec, for parallel and perpendicular to the grain: (1) the average value of f_{emb} increased by 25.2% and 30.1%, respectively, (2) the characteristic value of f_{emb} increased by 22.9% and 28.7%, respectively, and (3) K_{el} increased by 11.9% and 35.5%, respectively. On the other hand, the parallel to grain ductility value Δ decreased by 15.6% between failure occurring in 300 sec and 0.3 sec. Given that the embedment properties and ductility are important parameters influencing the behaviour and capacity of timber connections, such significant differences have consequences on the design of connections. Therefore, the strain rate cannot be ignored in connections subjected to extreme dynamic events. This is further illustrated later in this results section.

Typical failure modes of the embedment tests are shown in Figure 18. For loading parallel to the grain, cracks eventually initiated directly under the dowel and propagated until they reached the base of the samples. On the other hand, cracks developed from the sides of the samples when loaded perpendicular to the grain and propagated along the grain direction at large deformation.

Fracture energy (Mode I)

The stress-displacement curves resulting from the fracture energy Mode I tests under all strain rates are shown in Figure 19. Loading speeds and average failure times, maximum stresses and fracture energies, with associated CoV, are summarised in Table 2. The characteristic fracture energies are also provided in Table 2.

One-way ANOVA analyses showed that (1) there were no statistically significant differences between the fracture energies of the 300 sec, 30 sec and 3 sec targeted failure group means ($F(2,57) = 0.149$, $p = 0.86$) and (2) there was a statistically significant difference between the mean of all four groups ($F(3,76) = 7.70$, $p = 1.4\times10^{-4}$). Therefore, the average Mode I fracture energy seems to only be affected by the strain rate from failure occurring at high strain rate. The change in average fracture energy between failure occurring in 3 sec and 0.3 sec is of 26.7%. However, as the variability in the fracture energy test results increases with the strain rate, the characteristic fracture energy decreases with increasing strain rate, as shown in Table 2.

Typical failure modes of the fracture energy Mode I tests are shown in Figure 20. All cracks initiated at the designated location (i.e., above the middle groove of each sample).

Fracture energy (Mode II)

The stress-displacement curves resulting from the fracture energy Mode II tests are shown in Figure 21 for all strain rates. Loading speeds and average failure times, maximum stresses and fracture energies, with associated CoV, are summarised in Table 3. The characteristic fracture energies are also provided in the table. Sixty-nine out of the 80 samples exhibited simultaneous shear failure above both grooves (Figure 22 (a)), while the remaining samples failed first on one side, then tilted and ultimately failed on both sides (Figure 22 (b)), which resulted in local maxima in the stress-displacement curves (Figure 21). The results from both failure modes were analysed together.

A one-way ANOVA analysis showed that there were no statistically significant differences between the fracture energies of all strain rate group means ($F(3,76) = 0.87$, $p = 0.45$). Additionally, and contrary to Mode I, the characteristic fracture energies for Mode II were not affected by the strain rate.

Tension perpendicular to grain

The loading speeds, average failure times and tensile capacities for the tension perpendicular to grain tests are summarised in Table 4. A one-way ANOVA analysis showed that there were no statistically significant differences between the tensile strength of all strain rate group means ($F(3,76) = 0.27$, $p = 0.84$). The characteristic values were also independent of the strain rate and therefore, the tensile strength perpendicular to the grain for the analysed LVL was found to be insensitive to the investigated range of strain rates. Note that as timber is known to be sensitive to the so-called size effect (Isaksson, 2003) and the stressed volume in the present tests is small, extrapolating the test results to full size members needs further examination.

Timber connections

Design equations in Eurocode

Figure 23 plots the influence of the strain rate on the capacity of the single shear connection type using the Eurocode 5 design equations for Member 2 (Figure 11) loaded parallel (Figure 23 (a)) and perpendicular to the grain (Figure 23 (b)). The design capacity increased significantly by up to 22.9% and 26.9% for Member 2 loaded parallel and perpendicular to grain, respectively, from failure occurred in 300 sec to 0.3 sec. For both static and dynamic, single shear connections are predicted to fail for low value of t_2 due to the rigid rotation of the dowel and local bearing failure of the timber members (Eq. (4)) to eventually change as t_2 increases to either one (Eq. (6)) or two (Eq. (7)) plastic hinges developing in the dowel. For double shear connections, failure is predicted to occur due to bearing failure of Member 2 under the dowel (Eq. (10)) for low value of t_2 to change to three plastic hinges developing in the dowel (Eq. (7)) as t_2 increases. However, despite similar failure modes developing statically and dynamically, the design equations also predict that the change between the failure modes mentioned above can occur statically and dynamically at different value of t_2, a phenomenon which could potentially influence the overall ductility of the connections. For instance, for single shear connections and Member 2 loaded parallel to the grain, the design equations predict that the change between failure resulting of the rigid rotation of the dowel and local bearing failure of the timber members (Eq. (4)) and the intrinsically more ductile failure mode of two plastic hinges developing in the dowel (Eq. (7)) would occur for and t_2 = 85 mm statically and t_2 = 75 mm dynamically.

Similar to Figure 23, Figure 24 plots the influence of the strain rate on the capacity of the double shear connection type using the Eurocode 5 design equations for Member 2 loaded parallel (Figure 24 (a)) and perpendicular to the grain (Figure 24 (b)). Between failure occurring in 300 sec and 0.3 sec, the design capacity increased by up to 22.7% and 28.7% when Member 2 is loaded parallel and perpendicular to the grain, respectively. These values are similar to the single shear connection type. Different static and dynamic failure modes were also predicted for given configurations by the design equations.

Experimental tests

Figure 25 plots the load-displacement curves of the timber connections tested quasi-statically and dynamically. The average maximum forces, failure times and ductility values, with associated CoV, are summarised in Table 5. For Configuration #1, the dynamic capacity was 7.5% higher than the static capacity, however, the ductility significantly decreased by 32.5%. For Configuration #2, the dynamic capacity was significantly higher than the static one (29.9%), while the ductility decreased by 11.5%. The ductility percentage decrease for Configuration #2 is less than that for Configuration #1 and is mainly due to one of the static tests showing significantly less ductility than the other two (Figure 25 (b)). All connections statically and dynimically failed in a similar manner corresponding to embedment failure developing first with bending of the bolts (as predicted by the Eurocode 5 (EN 1995-1-1, 2004)), and slipping eventually occurring. The failure mode is shown in Figure 26.

Overall, the timber connection tests confirm the embedment test results and the capacities calculated from the Eurocode 5 design equations by proving that the behaviour of connections tested dynamically is different than that tested statically. As discussed in the introduction, this finding has profound consequences on the design of timber connections as the ductility level assumed in design, typically based on the static behaviour, may not be reached dynamically. During a seismic event, less energy than anticipated would be absorbed and premature failure of the connections can ensue. Additional tests on different connection configurations and timber materials are needed to better understand this phenomenon.

CONCLUSION

This study demonstrated that the strain rate can significantly influence the material properties which are controlling the behaviour of timber connections. For the strain rates experimentally investigated in this paper, corresponding to failure occurring between 300 sec (quasi-static) and 0.3 sec (dynamic – earthquake and progressive collapse events), and softwood LVL, the following results were found:

- The parallel and perpendicular to grain dynamic embedment strengths on 16 mm dowelled connections were 25.2% and 30.1% higher, respectively, than the quasi-static strengths. Similarly, the dynamic embedment stiffness increased by 11.9% (parallel) and 35.5% (perpendicular) when compared to the quasi-static behaviour.
- When loaded parallel to the grain, the embedment ductility of the dowelled connections decreased by 15.6% from failure occurring in 300 sec to 0.3 sec.

- For the strain rates investigated, the Mode II fracture energies and tension strengths perpendicular to the grain of the LVL material were found not to be affected by the strain rate.
- The Mode I average fracture energies were only affected by the strain at high strain rate (failure in 0.3 sec). However, due to the variability in the test results increasing with the strain rate, the characteristic Mode I fracture energy was found to decrease with increasing strain rate.

The above results have significant consequences on the design of timber connections subjected to dynamic loads. For earthquake design, if the ductility levels are obtained from the quasi-static behaviour, such levels may not be reached dynamically leading to unsafe designs. These consequences were further analysed in the paper and results showed that:

- Using the characteristic embedment strength values derived from the experimental data in the Eurocode 5 design equations, the design capacity of single and double shear connections can increase by up to 29% between failure occurring in 300 sec and 0.3 sec and different quasi-static and dynamic failure modes may develop. The latter can potentially result in different ductility levels.
- Experimental tests performed on bolted connections confirmed the different quasi-static and dynamic behaviour of timber connections. For the tested connections, the dynamic strength and ductility were found to be up to 30% higher and up to 32.5% lower than the quasi-static ones.

Additional tests are needed to better understand the dynamic behaviour of timber connections to ultimately develop safe design rules for earthquake and progressive collapse events.

DATA AVAILABILITY STATEMENT

Some or all data, models, or code that support the findings of this study are available from the corresponding author upon reasonable request.

REFERENCES

Ardalany, M., Deam, B., and Fragiacomo, M. (2012). "Experimental results of fracture energy and fracture toughness of Radiata Pine laminated veneer lumber (LVL) in mode I (opening)." *Materials and Structures*, 45(8), 1189-1205.

Ardalany, M., Deam, B., Fragiacomo, M., and Crews, K. I. "Tension perpendicular to grain strength of wood, Laminated Veneer Lumber (LVL), and Cross-Banded LVL (LVL-C)." *Proc., Proceedings of the 21st Australasian Conference on the Mechanics of Structures and Materials (ACMSM21)*, CRC Press/Balkema, 891 - 896.

AS 1720.1 (2010). "Timber structures, Part 1: Design methods." Standards Australia, Sydney, Australia.

AS 4100 (2020). "Steel Structures." Standards Australia, Sydney, Australia.

AS/NZS 1080.1 (2012). "Timber - Methods of test - Moisture content." Standards Australia, Sydney, Australia.

ASTM D143-14 (2014). "Standard Test Methods for Small Clear Specimens of Timber." ASTM International, Pennsylvania, USA.

ASTM D5764 − 97a (2018). "Standard Test Method for Evaluating Dowel-Bearing Strength of Wood and Wood-Based Products." ASTM International, Pennsylvania, USA.

Bischoff, P. H., and Perry, S. H. (1991). "Compressive behaviour of concrete at high strain rates." *Materials and Structures*, 24(6), 425-450.

Bragov, A., and Lomunov, A. K. (1997). "Dynamic properties of Some Wood Species." *Journal de Physique IV*, 07(C3), C3-487-C483-492.

Brühl, F., Kuhlmann, U., and Jorissen, A. (2011). "Consideration of plasticity within the design of timber structures due to connection ductility." *Engineering Structures*, 33(11), 3007-3017.

Carter Holt Harvey (2015). "Futurebuild LVL specific engineering design guide." Carter Holt Harvey Woodproducts.

Cheng, X., Gilbert, B. P., Guan, H., Dias-da-Costa, D., and Karampour, H. (2022). "Influence of the earthquake and progressive collapse strain rate on the structural response of timber dowel type connections through finite element modelling." *Journal of Building Engineering*, 57, 104953.

Cheng, X., Gilbert, B. P., Guan, H., Underhill, I. D., and Karampour, H. (2021). "Experimental dynamic collapse response of post-and-beam mass timber frames under a sudden column removal scenario." *Engineering Structures*, 233, 111918.

Conrad, M. P. C., Smith, G. D., and Fernlund, G. (2003). "Fracture of Solid Wood: A Review of Structure and Properties at Different Length Scales " *Wood and Fiber Science*, 35(4), 570–584.

Ellingwood, B. R., Smilowitz, R., Dusenberry, D. O., Duthinh, D., Lew, H. S., and Carino, N. J. (2007). "Best practices for reducing the potential for progressive collapse in buildings - NISTIR 7396."

EN 383 (2007). "Timber structures – Test methods. Determination of embedding strength and foundation values for dowel type fasteners." The European Union Per Regulation, Brussel, Belgium.

EN 1995-1-1 (2004). "Eurocode 5: Design of timber structures - Part 1-1: General - Common rules and rules for buildings ", The European Union Per Regulation, Brussel, Belgium.

EN 14358 (2016). "Timber structures - Calculation and verification of characteristic values." The European Union Per Regulation, Brussel, Belgium.

Franke, B., and Quenneville, P. (2014). "Analysis of the fracture behavior of Radiata Pine timber and Laminated Veneer Lumber." *Engineering Fracture Mechanics*, 116, 1-12.

Gharib, M., Hassanieh, A., Valipour, H., and Bradford, M. A. (2017). "Three-dimensional constitutive modelling of arbitrarily orientated timber based on continuum damage mechanics." *Finite Elements in Analysis and Design*, 135, 79-90.

Gilbert, B. P., Dias-da-Costa, D., Lebée, A., and Foret, G. (2020). "Veneer-based timber circular hollow section beams: Behaviour, modelling and design." *Construction and Building Materials*, 258, 120380.

Gilbert, B. P., Fernando, D., and Pham, C. H. (2022). "Experimental techniques in structural Testing: Common Mistakes, how to avoid them and other advice." *Structures*, 41, 1687-1699.

Gilbert, B. P., Husson, J. M., Bailleres, H., McGavin, R. L., and Fischer, M. F. (2018). "Perpendicular to grain and shear mechanical properties of veneer-based elements glued from single veneer sheets recovered from three species of juvenile subtropical hardwood plantation logs." *European Journal of Wood and Wood Products*, 76(6), 1637-1652.

Gilbertson, C. G., and Bulleit, W. M. (2013). "Load Duration Effects in Wood at High Strain Rates." *ASCE Journal of Materials in Civil Engineering*, 25(11), 1647-1654.

Harte, A. M. (2017). "Mass timber – the emergence of a modern construction material." *Journal of Structural Integrity and Maintenance*, 2(3), 121-132.

Isaksson, T. (2003). "Structural timber - Variability and statistical modelling (Chapter 4)." *Timber Engineering*, S. Thelandersson, and H. J. Larsen, eds., Wiley and Sons, England.

Jacques, E., Lloyd, A., Braimah, A., Saatcioglu, M., Doudak, G., and Abdelalim, O. (2014). "Influence of high strain-rates on the dynamic flexural material properties of spruce–pine–fir wood studs." *Canadian Journal of Civil Engineering*, 41(1), 56-64.

Johansen, K. W. (1949). "Theory of timber connection." *International Associ-ation for Bridge and Structural Engineering,*, 9, 249-262.

Jorissen, A., and Fragiacomo, M. (2011). "General notes on ductility in timber structures." *Engineering Structures*, 33(11), 2987-2997.

Keeton, J. R. (1968). "Dynamix properties of small, clear specimens of structural grade timber." Defense Technical Information Centre, U.S.A.

Knott, J. F. (1973). *Fundementals of fracture mechanics*, Butterworths.

Kuzmanovska, I., Gasparri, E., Tapias Monné, D., and Aitchison, M. "Tall timber buildings: emerging trends and typologies." *Proc., 2018 World Conference on Timber Engineering*, Electronic proceedings.

Larsen, H. J., and Gustafsson, P. J. "The fracture of wood in tension perpendicular to the grain results from a joint testing project." *Proc., 23rd CIB W18 Meeting*.

Lyu, C. H., Gilbert, B. P., Guan, H., Underhill, I. D., Gunalan, S., Karampour, H., and Masaeli, M. (2020). "Experimental collapse response of post-and-beam mass timber frames under a quasi-static column removal scenario." *Engineering Structures*, 213, 110562.

Mai, Y. W. (1975). "On the velocity-dependent fracture toughness of wood." *Wood Science and Technology*, 8(1), 364–367.

McGavin, R. L., Nguyen, H. H., Gilbert, B. P., Dakin, T., and Faircloth, A. (2019). "A comparative study on the mechanical properties of laminated veneer lumber (LVL) produced from blending various wood veneers,." *BioResources*, 14(4), 9064-9081.

Nadeau, J. S., Bennett, R., and Fuller, E. R. (1982). "An explanation for the rate-of-loading and the duration-of-load effects in wood in terms of fracture mechanics." *Journal of Materials Science*, 17(10), 2831-2840.

Nouri, F., Valipour, H. R., and Bradford, M. A. (2019). "Finite element modelling of steel-timber composite beam-to-column joints with nominally pinned connections." *Engineering Structures*, 201, 109854.

Reid, S. R., and Peng, C. (1997). "Dynamic uniaxial crushing of wood." *International Journal of Impact Engineering*, 19(5), 531-570.

Rothoblaas (2019). "Plates and connectors for timber buildings, structures and outdoor." 54-59.

Schniewind, A. P., and Pozniak, R. A. (1971). "On the fracture toughness of Douglas fir wood." *Engineering Fracture Mechanics*, 2(3), 223-230.

Sreenivasan, P. R., and Ray, S. K. (2001). "Mechanical Testing at High Strain Rates." *Encyclopedia of Materials: Science and Technology*, K. H. J. Buschow, R. W. Cahn, M. C. Flemings, B. Ilschner, E. J. Kramer, S. Mahajan, and P. Veyssière, eds., Elsevier, Oxford, 5269-5271.

Stanzl-Tschegg, S. E., and Navi, P. (2009). "Fracture behaviour of wood and its composites. A review COST Action E35 2004–2008: Wood machining – micromechanics and fracture %J." *Holzforschung*, 63(2), 139-149.

Vasić, S., Ceccotti, A., Smith, I., and Sandak, J. (2009). "Deformation rates effects in softwoods: Crack dynamics with lattice fracture modelling." *Engineering Fracture Mechanics*, 76(9), 1231-1246.

Vasic, S., and Smith, I. (2002a). "Bridging crack model for fracture of spruce." *Engineering Fracture Mechanics*, 69(6), 745-760.

Vasic, S., Smith, I., and Landis, E. (2002b). "Fracture zone Characterization—Micro-Mechanical Study " *Wood and Fiber Science*, 34(1), 42-56.

Widehammar, S. (2004). "Stress-strain relationships for spruce wood: Influence of strain rate, moisture content and loading direction." *Experimental Mechanics*, 44(1), 44-48.

Wood, L. W. (1951). "Relation of strength of wood to duration of load." F. P. Laboratory, ed., United States Department of Agriculture, Forest service.

Wouts, J., Haugou, G., Oudjene, M., Coutellier, D., and Morvan, H. (2016). "Strain rate effects on the compressive response of wood and energy absorption capabilities – Part A: Experimental investigations." *Composite Structures*, 149, 315-328.

Xie, Q., Zhang, L., Zhang, B., Yang, G., and Yao, J. (2020). "Dynamic parallel-to-grain compressive properties of three softwoods under seismic strain rates: tests and constitutive modeling." *Holzforschung*, 74(10), 927-937.

Xu, B. H., Taazount, M., Bouchaïr, A., and Racher, P. (2009). "Numerical 3D finite element modelling and experimental tests for dowel-type timber joints." *Construction and Building Materials*, 23(9), 3043-3052.

Zhou, S. C., Demartino, C., and Xiao, Y. (2020). "High-strain rate compressive behavior of Douglas fir and glubam." *Construction and Building Materials*, 258, 119466.

Table 1: Embedment strength test results

Loading direction	Number of tests	Loading speed (mm/min)	T_f		K_{el}		$f_{y,5\%}$		f_{emb}			Δ	
			Average (s)	CoV (%)	Average (MPa/mm)	CoV (%)	Average (MPa)	CoV (%)	Average (MPa)	CoV (%)	Characteristic (MPa)	Average (mm)	CoV (%)
Parallel	20	0.6	318	17.4	131.8	19.2	40.5	8.8	42.5	7.5	36.7	3.2	17.4
	20	6	32.2	19.5	133.1	18.4	46.2	7.6	47.5	6.6	41.7	3.2	19.6
	20	60	3.0	21.5	152.2	16.9	47.7	7.4	50.2	6.6	44.2	2.9	21.6
	20	600	0.32	18.4	147.5	20.9	51.7	8.3	53.2	8.5	45.1	2.7	21.9
Perpendicular	20	1	300	N/A[(1)]	24.8	6.9	25.9	6.3	33.9	6.9	29.6	N/A	
	20	10	30		28.3	9.4	29.6	8.3	38.1	8.7	32.1		
	20	100	3		30.2	10.7	34.0	8.7	42.6	8.1	36.1		
	20	1,000	0.3		33.6	6.7	34.6	7.9	44.1	7.5	38.1		

[(1)]: For all perpendicular to grain embedment tests, no load drop was encountered before a 5 mm displacement. The failure time was then equal to the time at 5 mm displacement which is the same for all tests as the machine was driven in displacement control.

Table 2: Fracture energy Mode I test results

Number of tests	Loading speed (mm/min)	T_f		σ_{max}		G_{fI}		
		Average (s)	CoV (%)	Average (MPa)	CoV (%)	Average (N/mm)	CoV (%)	Characteristic (N/mm)
20	6	287	28.4	0.15	13.9%	1.17	15.8%	0.85
20	60	30.8	29.4	0.14	16.7%	1.21	20.5%	0.79
20	600	2.2	28.3	0.15	15.1%	1.16	30.4%	0.59
20	4,800	0.22	22.9	0.14	18.1%	0.85	31.6%	0.41

Table 3: Fracture energy Mode II test results

Number of tests	Loading speed (mm/min)	T_f		σ_{max}		G_{fI}		
		Average (s)	CoV (%)	Average (MPa)	CoV (%)	Average (N/mm)	CoV (%)	Characteristic (N/mm)
20	0.8	347	37.7	5.0	18.8	6.4	21.6	4.1
20	8	27.1	36.7	6.1	13.5	6.6	20.1	4.3
20	80	2.1	30.1	6.3	9.6	6.1	26.6	3.5
20	800	0.29	14.6	4.7	11.7	5.9	21.4	3.7

Table 4: Tension perpendicular to grain test results

Number of tests	Loading speed (mm/min)	T_f		$f_{t,90}$		
		Average (s)	CoV (%)	Average (MPa)	CoV (%)	Characteristic (MPa)
20	0.21	248	20.0	1.62	21.1	0.46
20	2.1	29.6	15.1	1.69	20.1	0.51
20	21	2.9	13.7	1.59	23.3	0.44
20	210	0.29	10.7	1.64	24.0	0.47

Table 5: Timber connection experimental test results

Connection	Loading speed type	T_f		F_{max}		Δ	
		Average (s)	CoV (%)	Average (kN)	CoV (%)	Average (mm)	CoV (%)
Configuration #1	Quasi-static	174.7	7.7	88.6	3.1	9.3	4.2
	Dynamic	0.151	18.6	95.2	5.7	6.3	19.9
Configuration #2	Quasi-static	129	22.4	68.4	5.4	6.2	26.3
	Dynamic	0.278	9.1	88.9	4.8	5.5	15.2

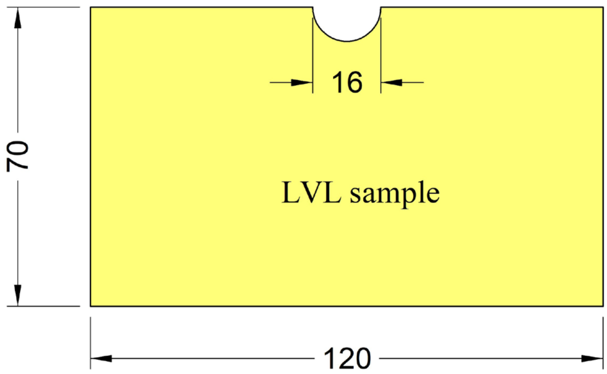

Figure 1: LVL sample dimensions for embedment tests (units in mm)

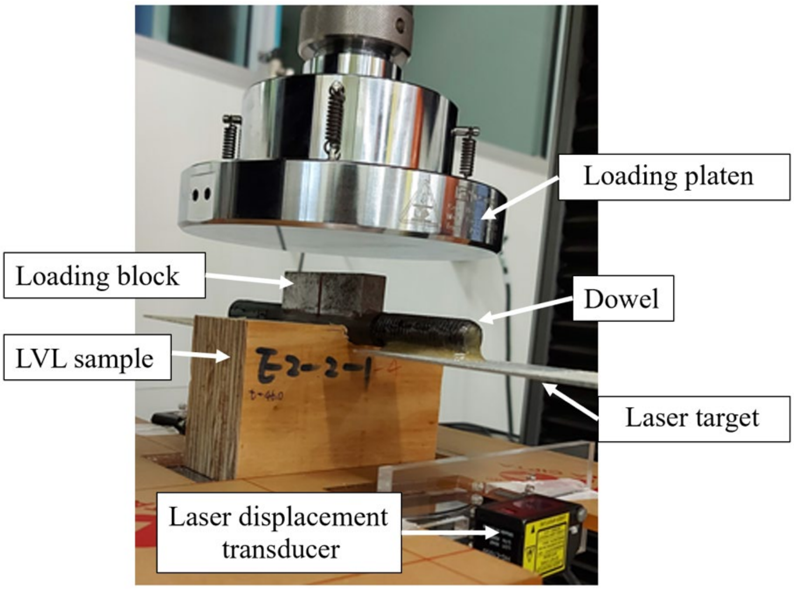

Figure 2: Embedment test setup

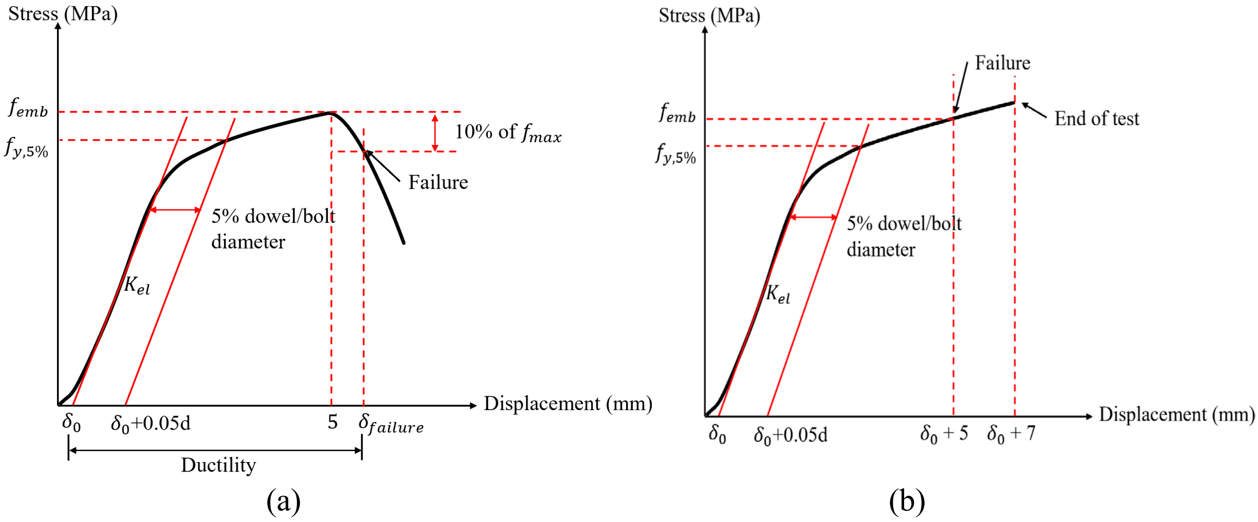

Figure 3: Embedment strength evaluation criteria for loading (a) parallel to grain and (b) perpendicular to grain

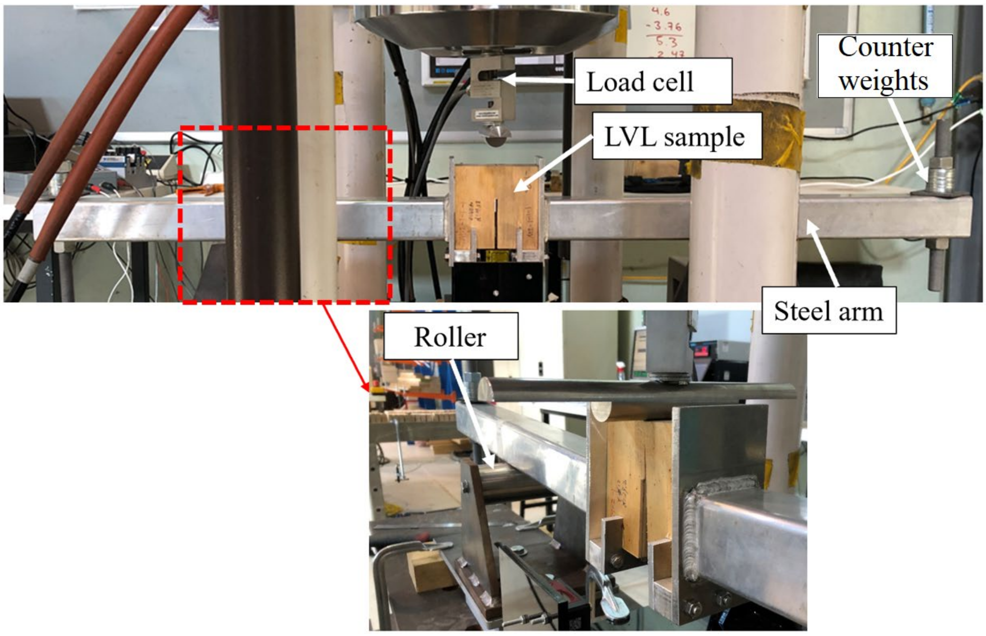

Figure 4: Mode I fracture test setup

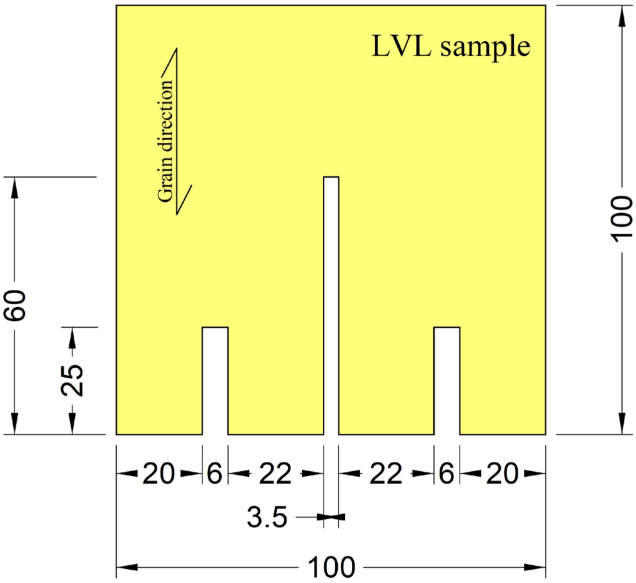

Figure 5: LVL sample dimensions for Mode I fracture tests (units in mm)

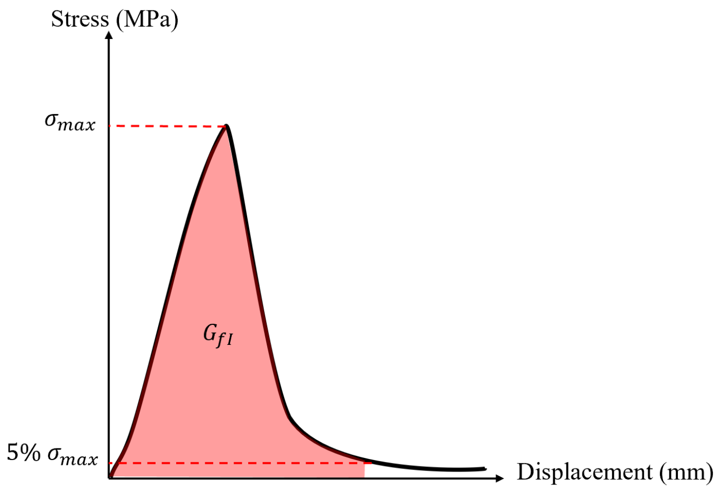

Figure 6: Mode I fracture test evaluation criteria

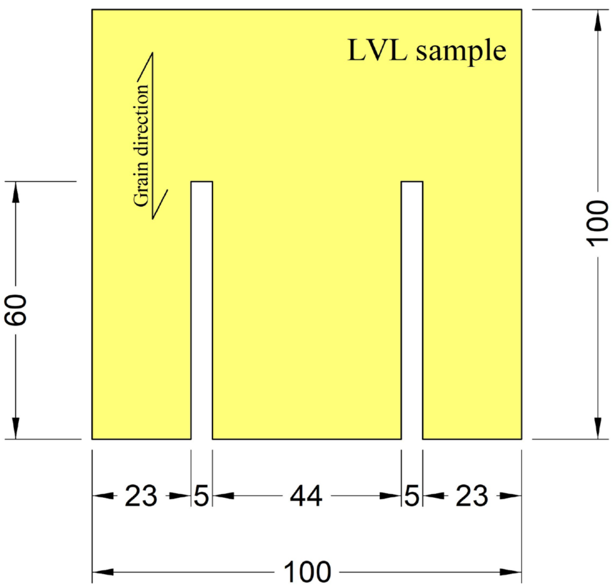

Figure 7: LVL sample dimensions for Mode II fracture tests (units in mm)

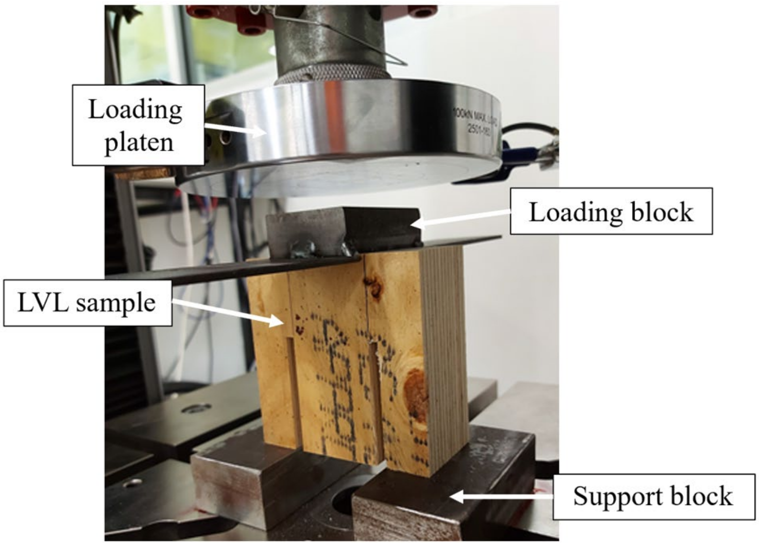

Figure 8: Mode II fracture test setup

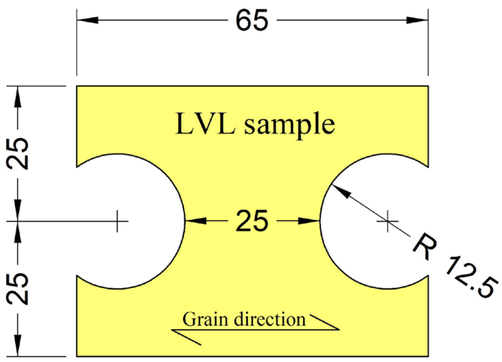

Figure 9: LVL sample dimensions for tension perpendicular to grain (units in mm)

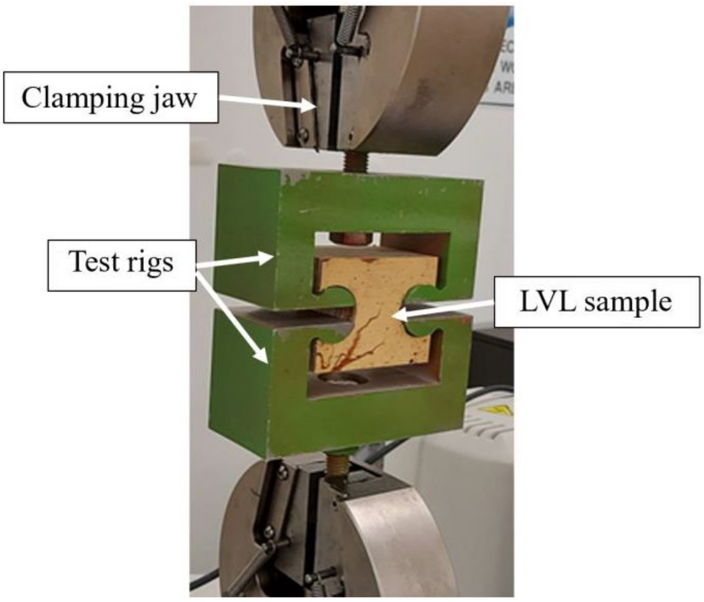

Figure 10: Tension perpendicular to grain test setup

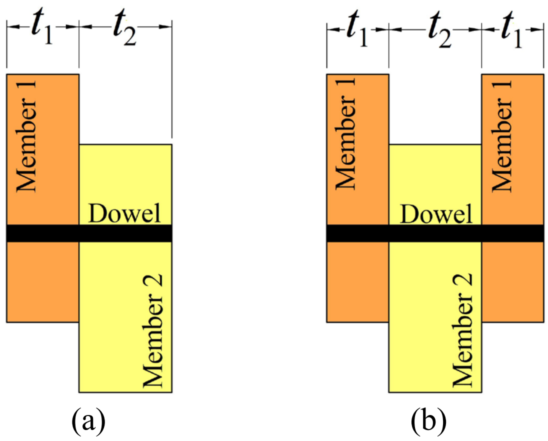

Figure 11: Timber-to-timber connection in (a) single and (b) double shear

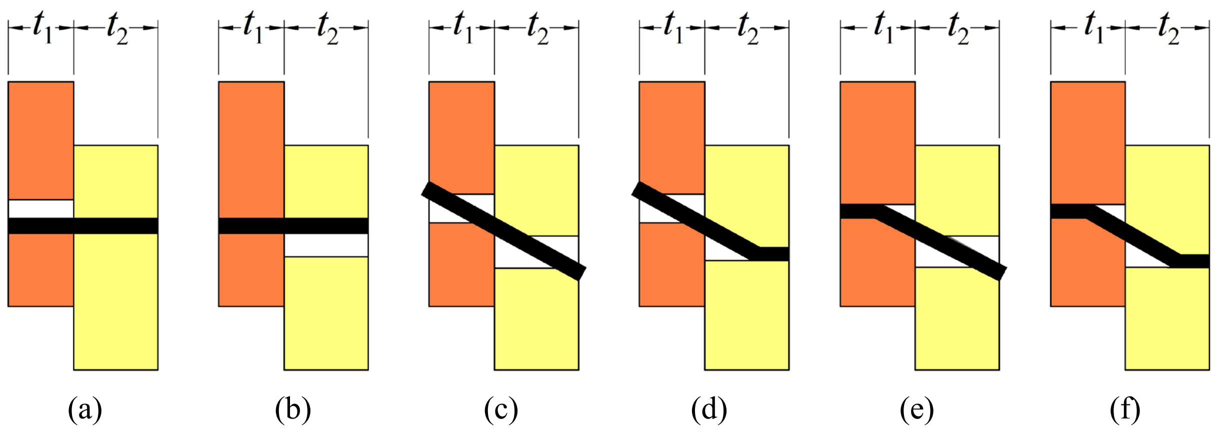

Figure 12: Failure modes reproduced from the Eurocode 5 (EN 1995-1-1, 2004) for a connection in single shear and corresponding to (a) Eq. (2), (b) Eq. (3), (c) Eq. (4), (d) Eq. (5), (e) Eq. (6) and (f) Eq. (7)

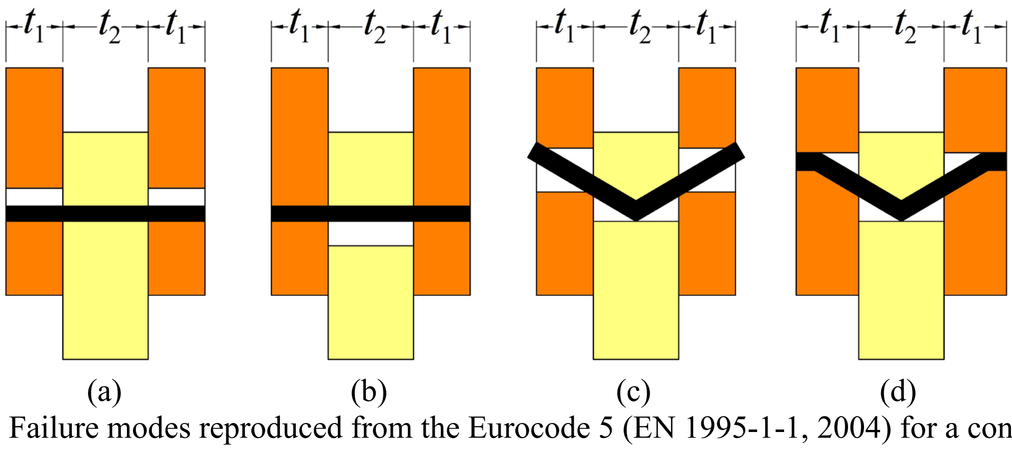

Figure 13: Failure modes reproduced from the Eurocode 5 (EN 1995-1-1, 2004) for a connection in double shear and corresponding to (a) Eq. (2), (b) Eq. (10), (c) Eq. (5) and (d) Eq. (7)

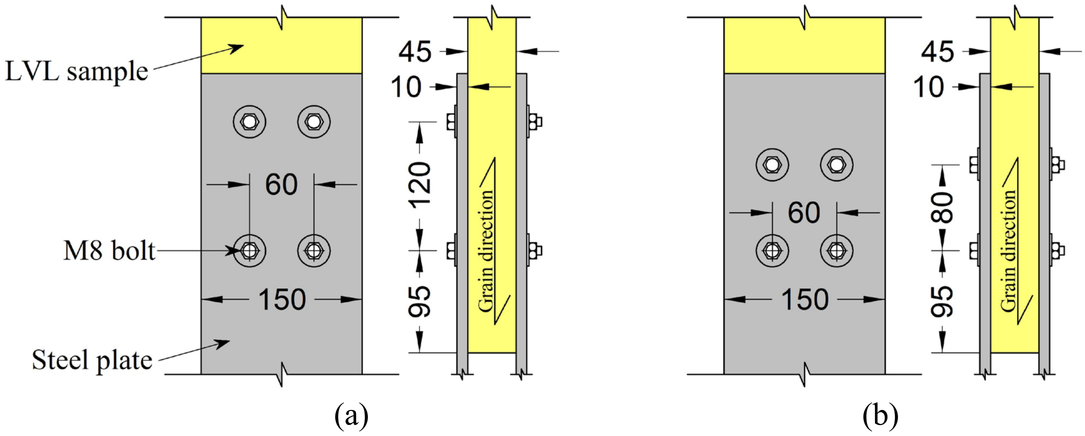

Figure 14: Timber connections, (a) Configuration #1 and (b) Configuration #2 (units in mm)

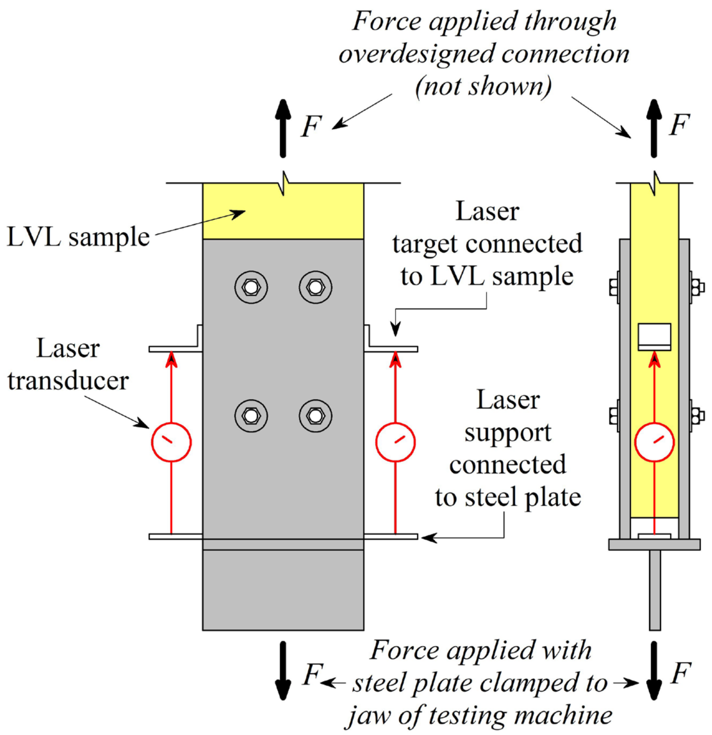

Figure 15: Timber connection test set-up

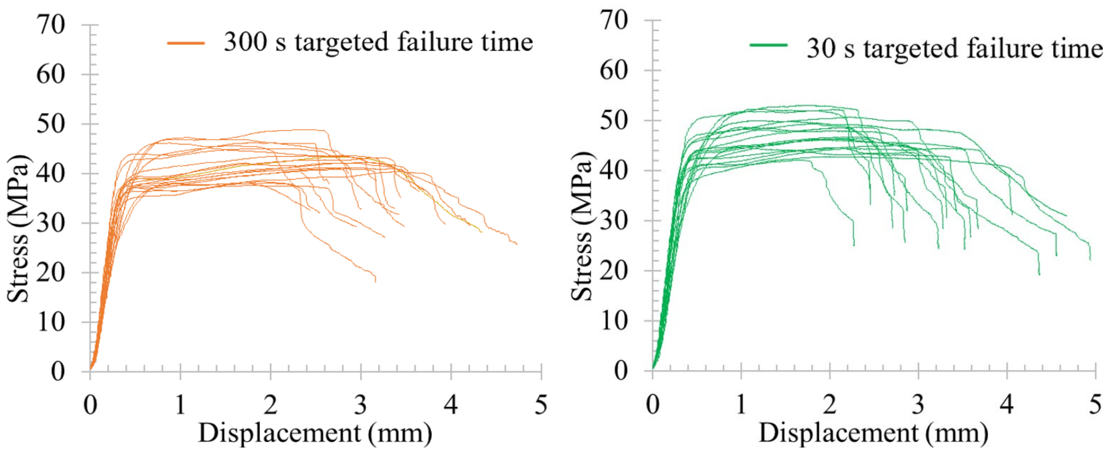

(a) (b)

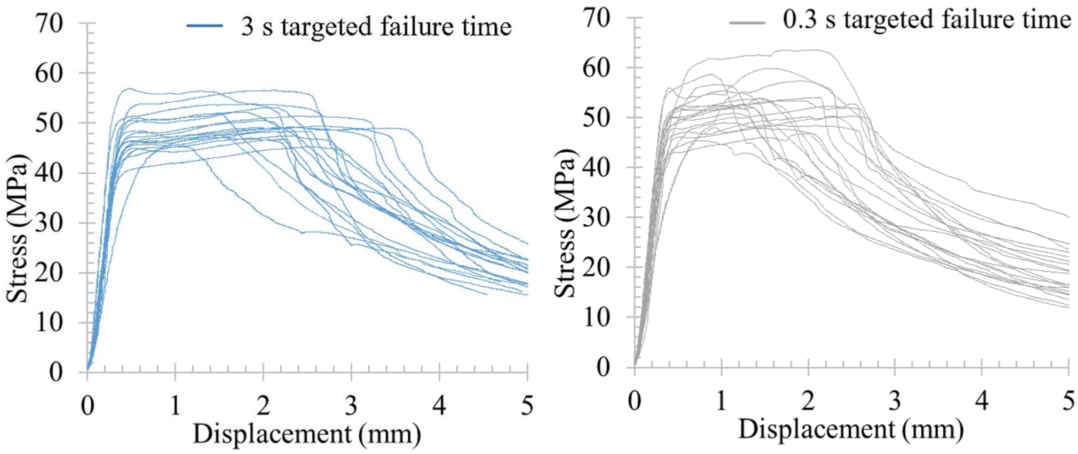

(c) (d)

Figure 16: Parallel to grain embedment test stress-displacement curves for targeted failure in (a) 300 sec, (b) 30 sec, (c) 3 sec and (d) 0.3 sec

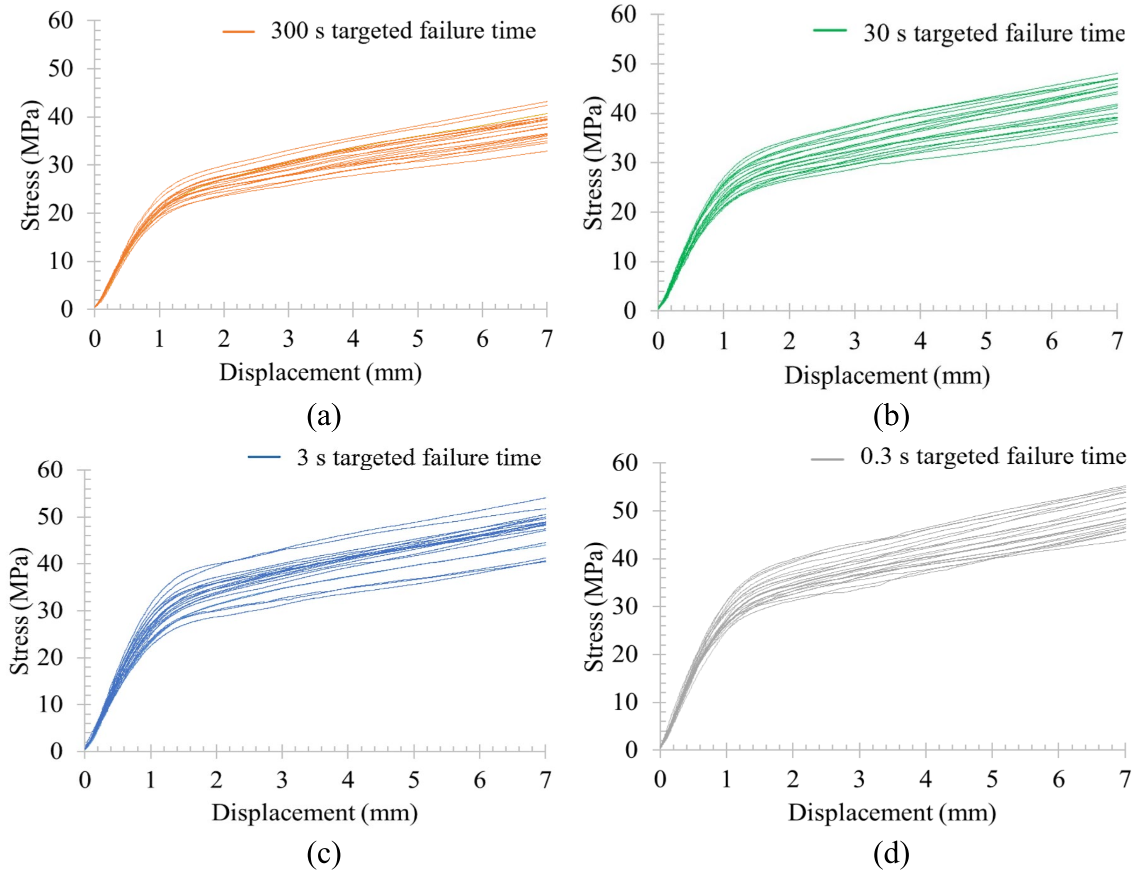

Figure 17: Perpendicular to grain embedment test stress-displacement curves for targeted failure in (a) 300 sec, (b) 30 sec, (c) 3 sec and (d) 0.3 sec

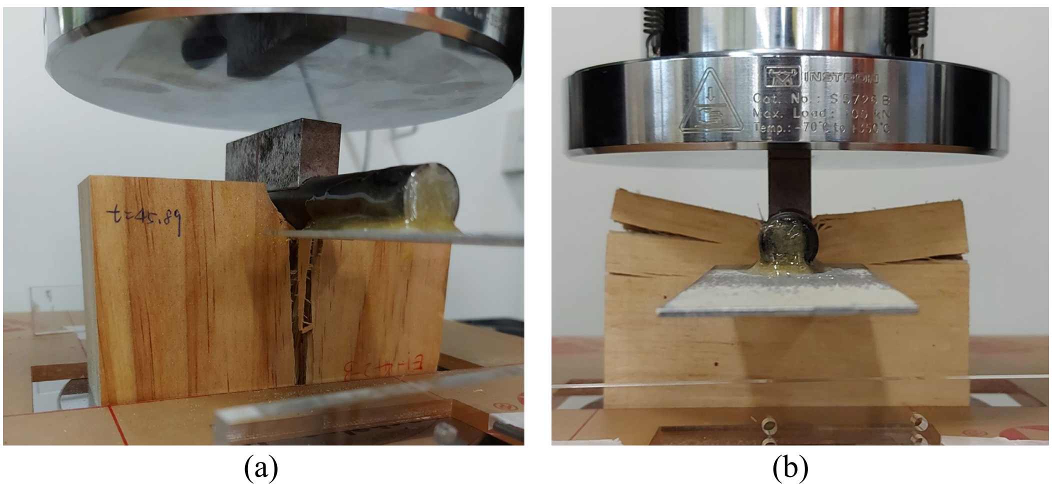

Figure 18: Embedment test failure modes at large deformation for loading (a) parallel and (b) perpendicular to grain

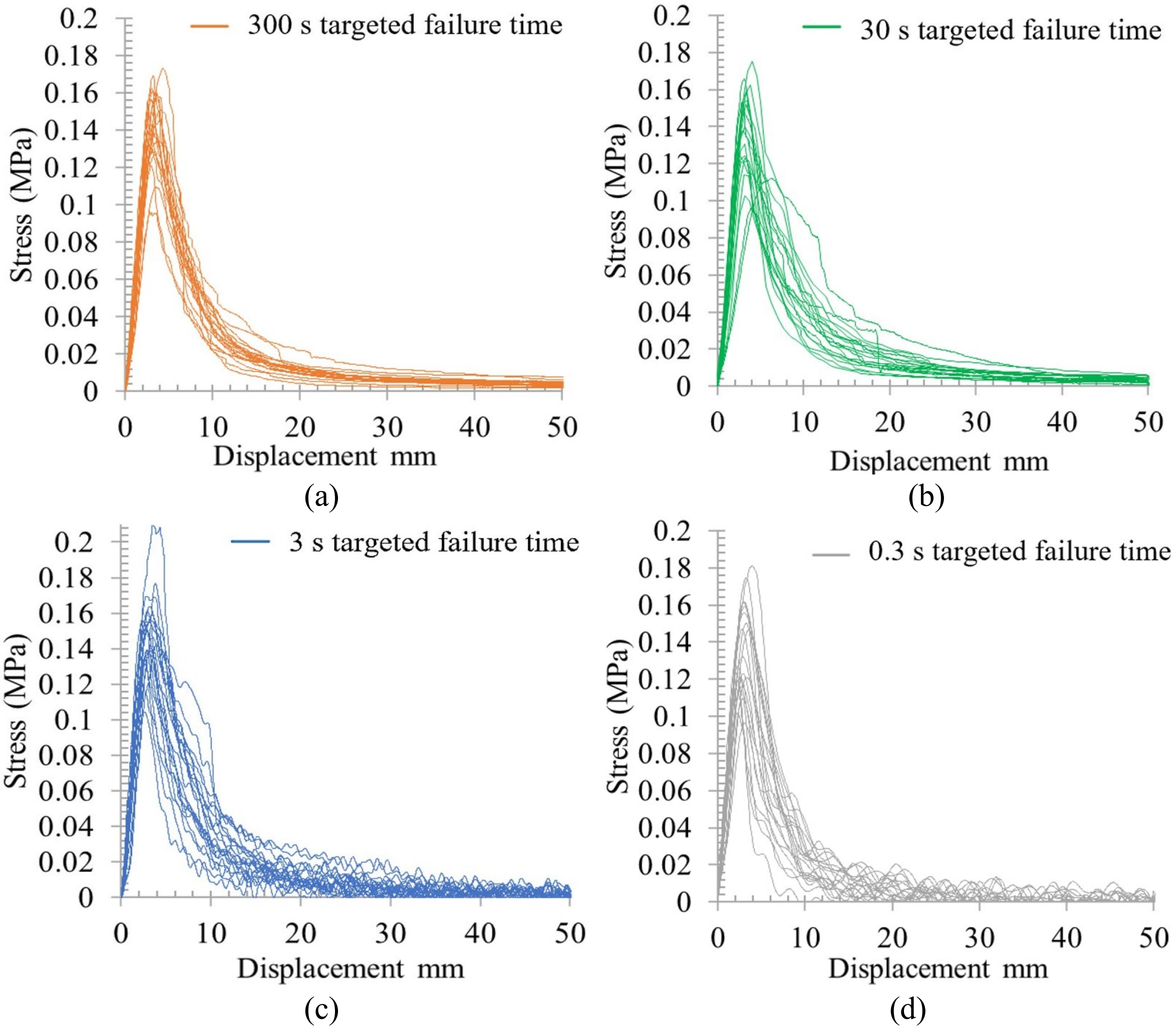

Figure 19: Fracture energy Mode I stress-displacement curves for targeted failure in (a) 300 sec, (b) 30 sec, (c) 3 sec and (d) 0.3 sec

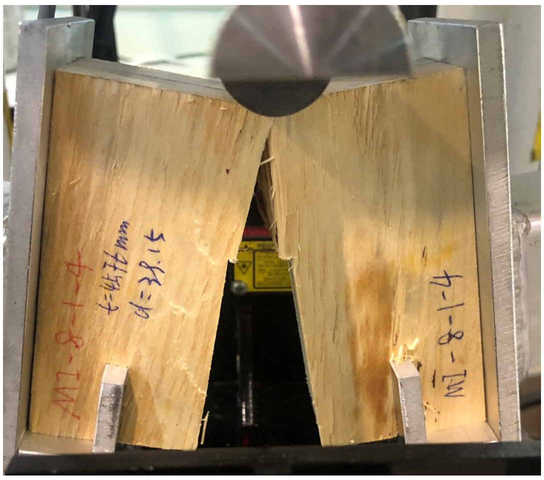

Figure 20: Fracture energy Mode I typical failure mode

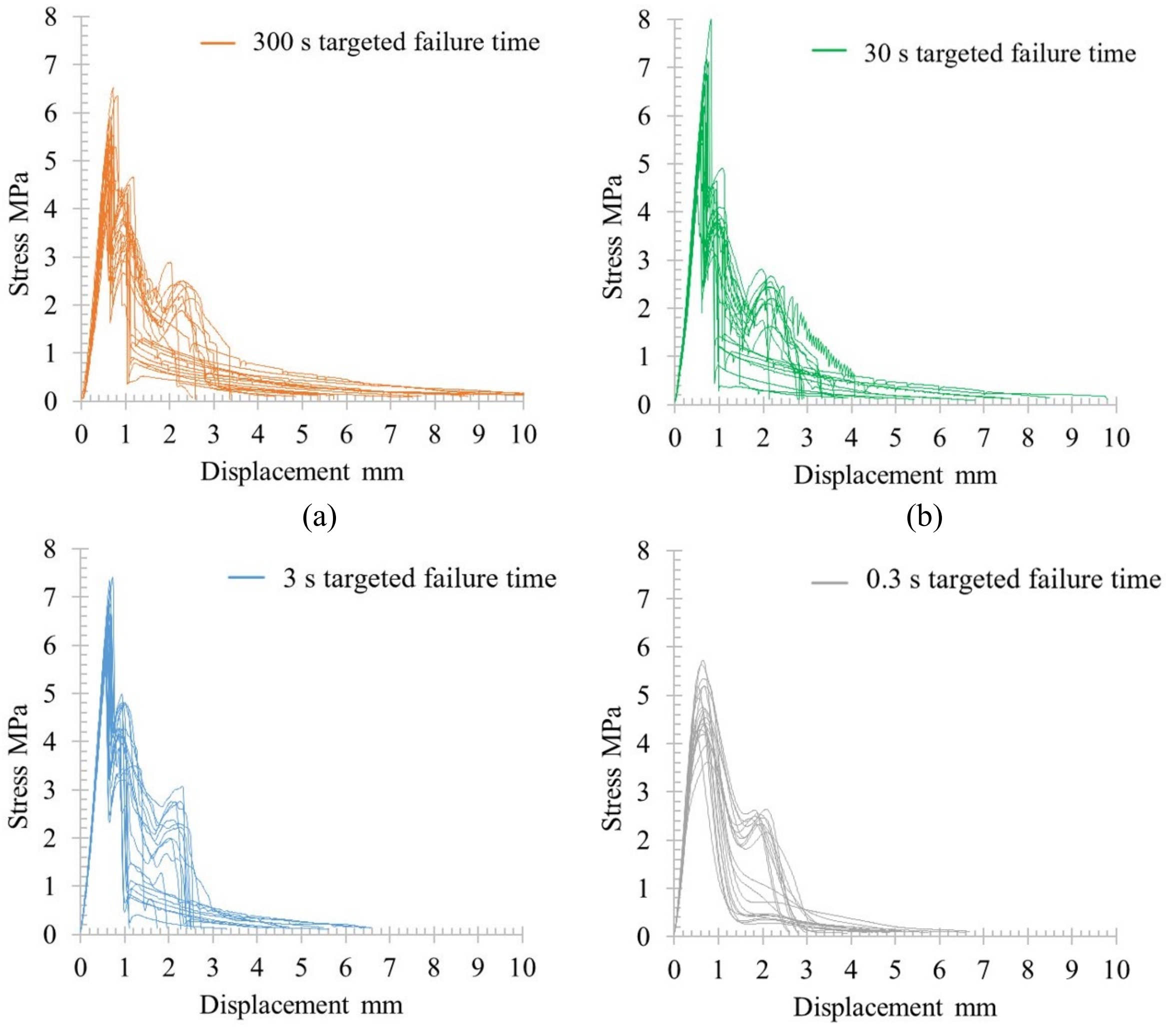

(c) (d)

Figure 21: Fracture energy Mode II stress-displacement curves for targeted failure in (a) 300 sec, (b) 30 sec, (c) 3 sec and (d) 0.3 sec

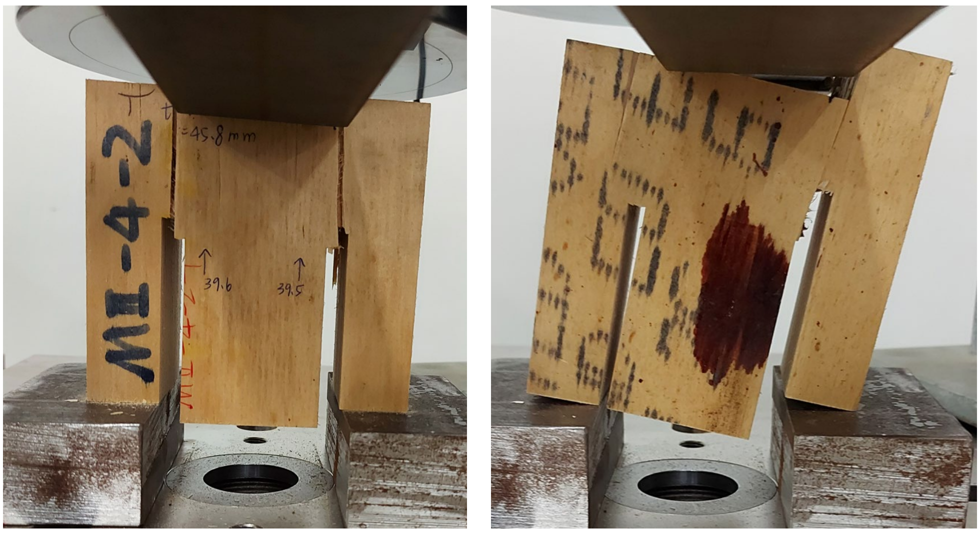

(a) (b)

Figure 22: Fracture energy Mode II (a) failure occurring above both grooves simultaneously and (b) failure occurring above one groove first

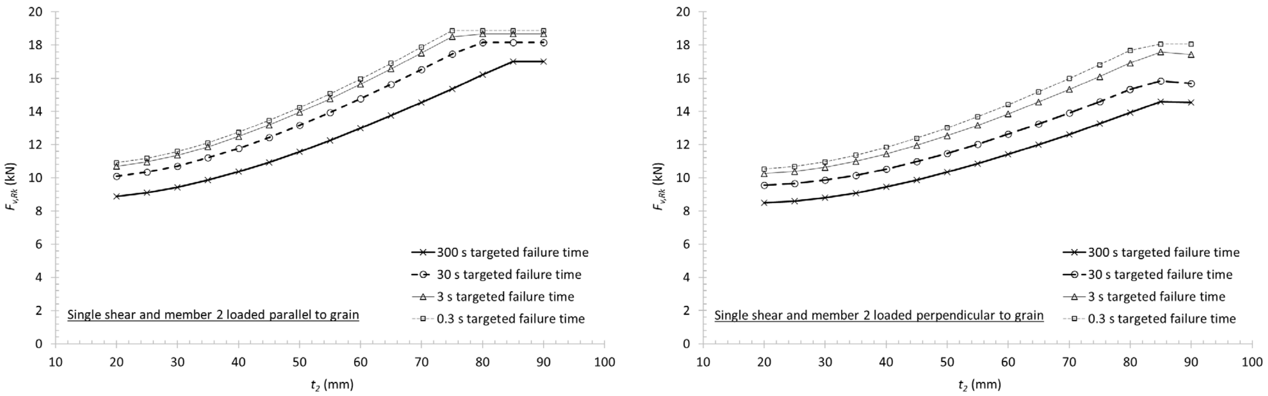

(a) (b)

Figure 23: Eurocode 5 design capacity of single shear connections versus Member 2 thickness (t_2) for various strain rates and Member 2 loaded (a) parallel to grain and (b) perpendicular to grain

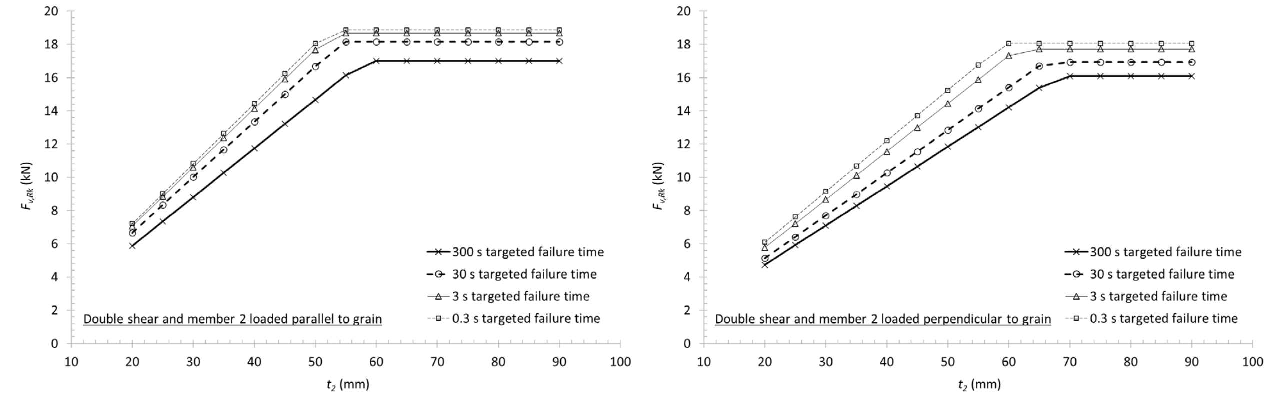

(a) (b)

Figure 24: Eurocode 5 design capacity of double shear connections versus Member 2 thickness (t_2)

for various strain rates and Member 2 loaded (a) parallel to grain and (b) perpendicular to grain

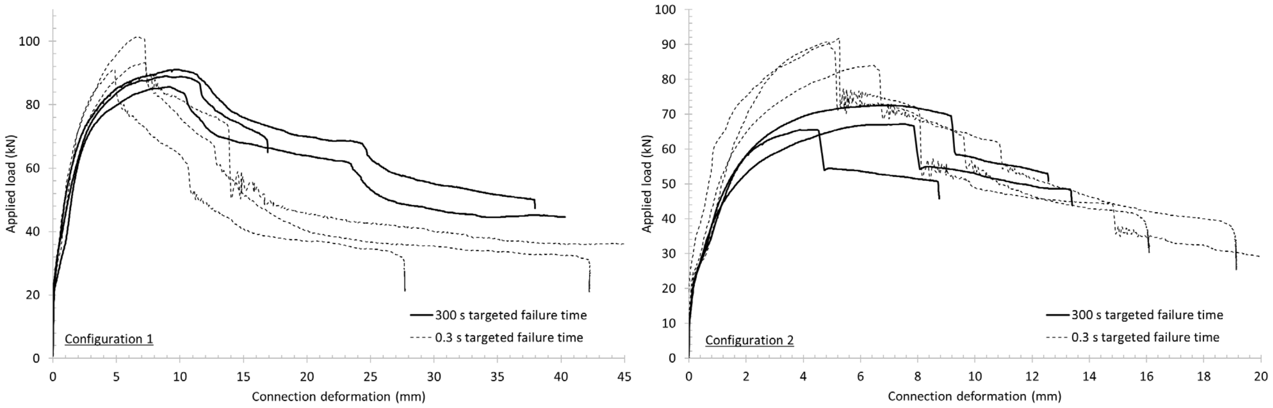

(a) (b)

Figure 25: Timber connection load-displacement curves for (a) Configuration #1 and (b) Configuration #2

Figure 26: Typical failure mode in timber connection, shown for Configuration #2